Supporting Material: Snowfall-albedo feedbacks could have led to deglaciation of Snowball Earth starting from mid-latitudes

Philipp de Vrese[1,*], Tobias Stacke[2], Jeremy Caves Rugenstein[3], Jason Goodman[4], and Victor Brovkin[1,5]

[1]Max Planck Institute for Meteorology, The Land in the Earth System, Hamburg, 20146, Germany
[2]Helmholtz-Zentrum Geesthacht, Institute of Coastal Research, Geesthacht, 21502, Germany
[3]Colorado State University, Department of Geosciences, Fort Collins, 80521, USA
[4]Wheaton College, Department of Physics and Astronomy, Norton, 02766, USA
[5]University of Hamburg, Center for Earth System Research and Sustainability, Hamburg, 20146, Germany
[*]philipp.de-vrese@mpimet.mpg.de

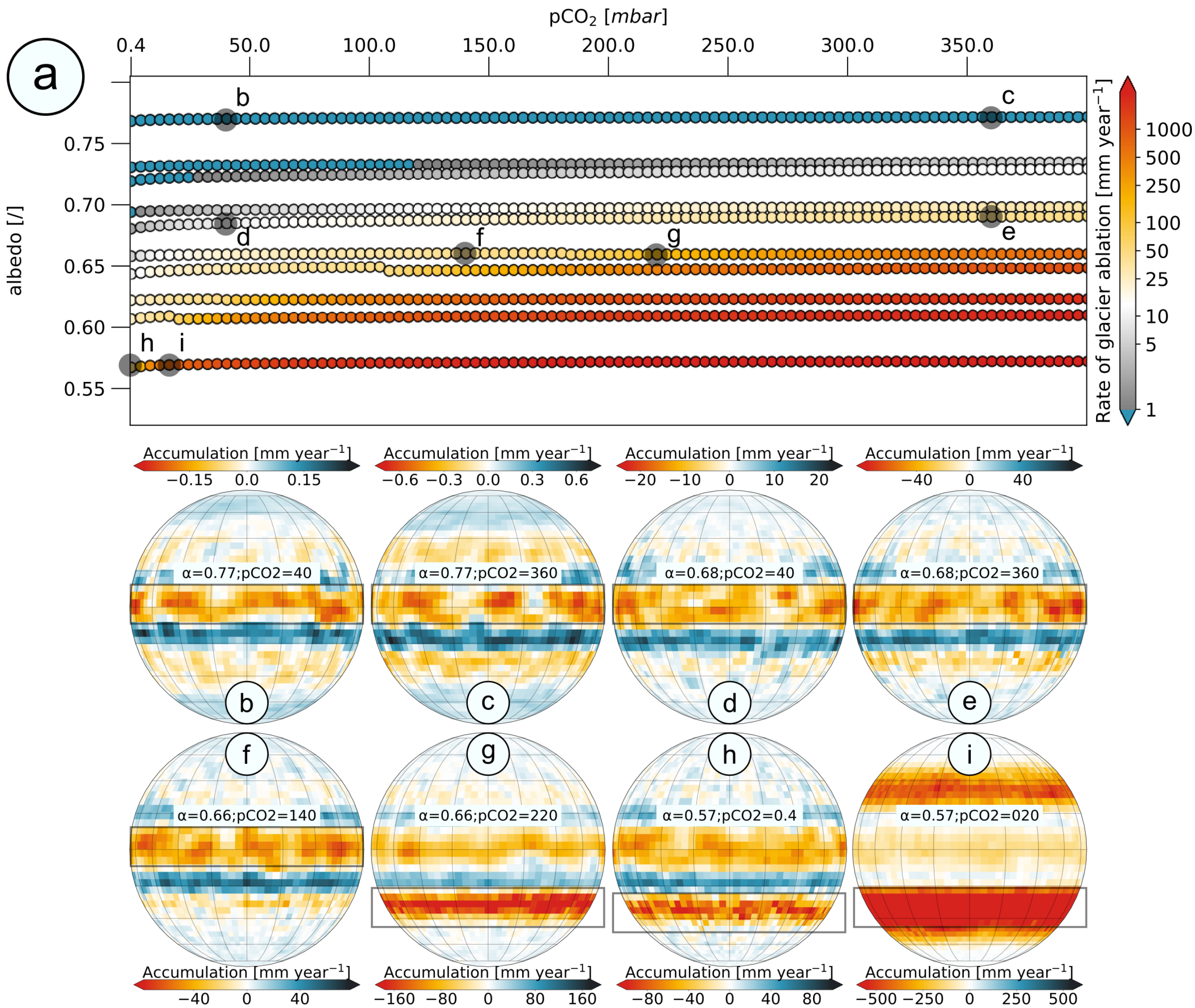

Supplementary Figure 1. Dependency of maximum ablation rates on surface albedo and atmospheric CO_2 concentrations

a) Simulated annual mean glacier ablation rates as a function of atmospheric CO_2 concentration (pCO_2) and surface albedo (α). Rates show the average over the 18.75°-wide latitudinal band (about 2000 km) in which maximum ablation rates were simulated. Grey circles indicate the combinations of α and pCO_2 that are presented in detail in sub-plots *b-i*. **b)** Rate of glacier accumulation simulated for $\alpha = 0.77$ and $pCO_2 = 40$ mbar. **c)** same as *b* but for $pCO_2 = 360$ mbar. **d)** same as *b* but for $\alpha = 0.68$ and $pCO_2 = 40$ mbar. **e)** same as *d* but for $pCO_2 = 360$ mbar. **f)** same as *b* but for $\alpha = 0.66$ and $pCO_2 = 140$ mbar. **g)** same as *f* but for $pCO_2 = 220$ mbar. **h)** same as *b* but for $\alpha = 0.57$ and $pCO_2 = 0.4$ mbar. **i)** same as *h* but for $pCO_2 = 20$ mbar. The simulations were carried out using the MPI-ESM1.2[1] with prescribed surface albedos (see sec. M1, M2). The grey boxes in sub-figurers *b-i* indicate the location of the latitudinal band where the maximum ablation rates are simulated. Note that color shading in panels b-i have variable ranges.

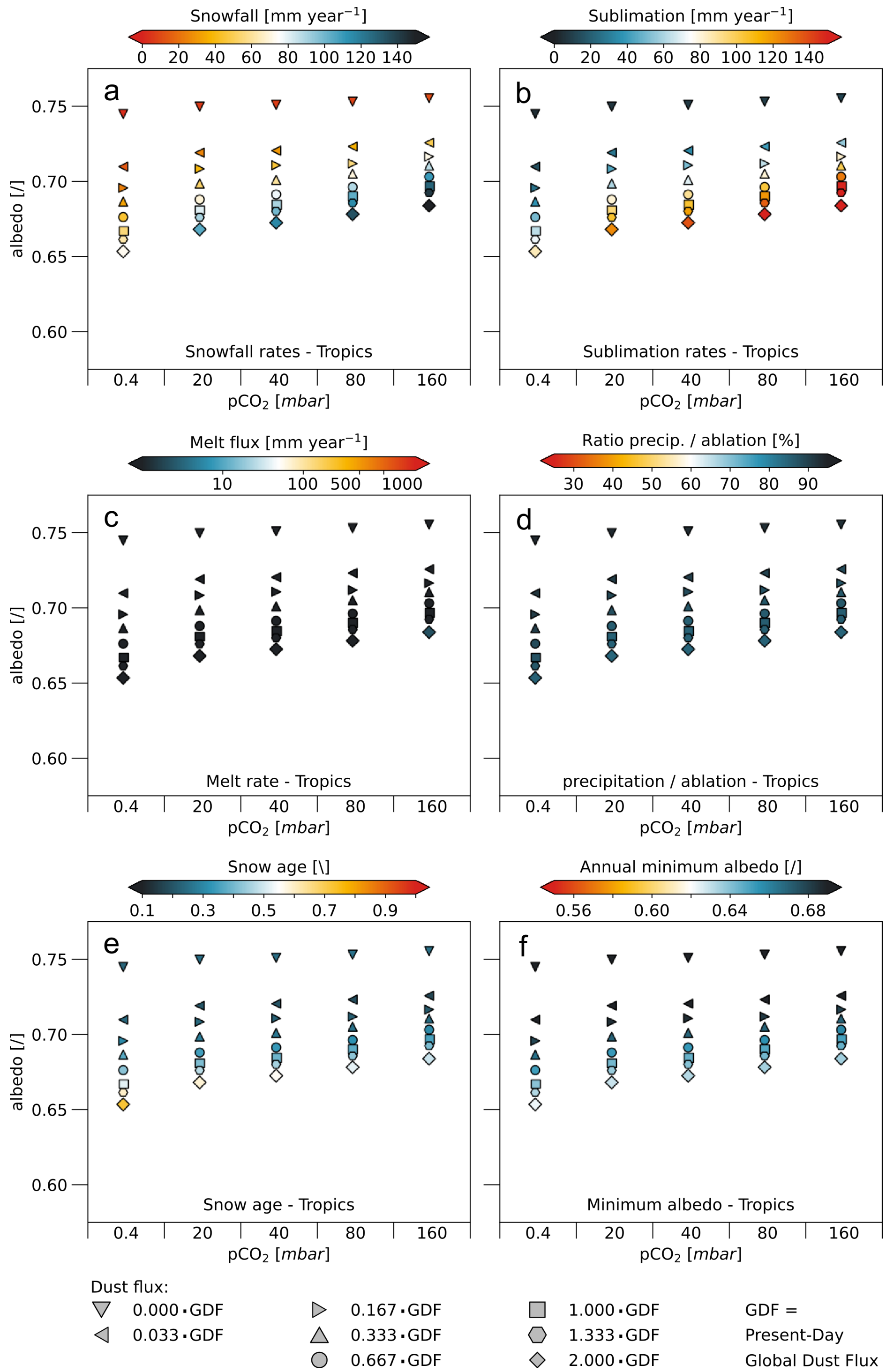

Supplementary Figure 2. Surface dynamics in the tropics for varying dust deposition rates and CO_2 levels
a) Simulated annual mean snowfall rates in the tropical ablation zone as a function of pCO_2, dust deposition fluxes and the resulting annual mean albedo. The values are representative for a 18.75°-wide latitudinal band in the equatorial regions between roughly 10.°N and 10.°S. **b)** Same as *a* but for sublimation. **c)** Same as *a* but for snow and ice melt. **d)** Same as *a* but for the ratio of precipitation and abltion, i.e. the sum of sublimation and melt flux. **e)** Same as *a* but for snow age, i.e. average of the snow ages of the main and the top-layer, weighted by the fraction that is exposed to the atmosphere. Note that the snow age is a dimensionless factor, where an age of 0 corresponds to fresh snow and an age of 1 to old, darkened snow. **f)** Same as *a* but showing the annual minimum albedo (monthly mean). The simulations were carried out using the MPI-ESM1.2[1] with an adapted snow-albedo scheme that estimates the albedo based on snow-age and surface temperatures and separates the snowpack into a top- and a main-layer (see sec. M1, M2).

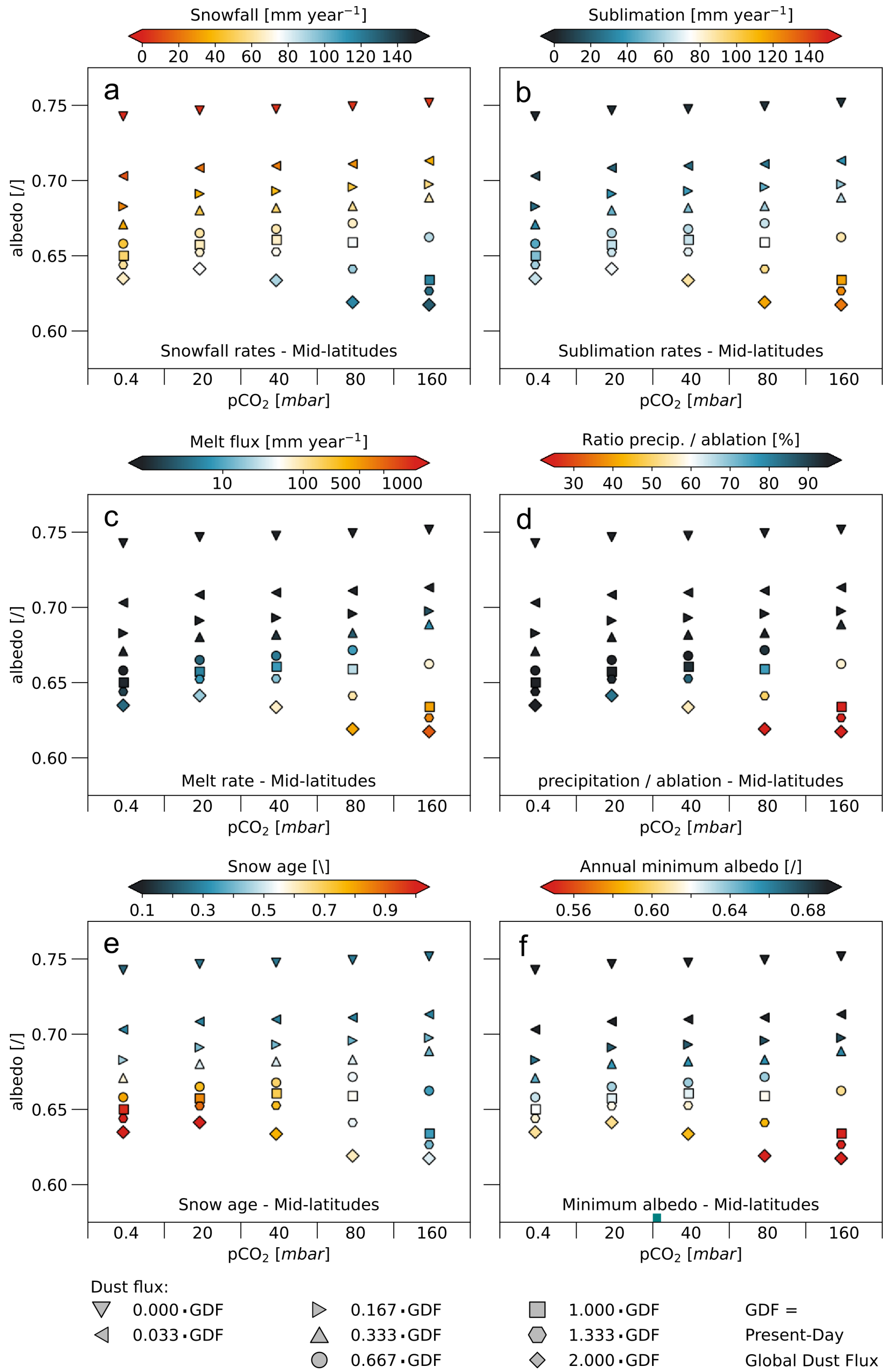

Supplementary Figure 3. Surface dynamics in the extratropics for varying dust deposition rates and CO_2 levels
Same as figure 2, but showing values representative of an 18.75°-wide latitudinal band roughly between 30.°S and 50.°S.

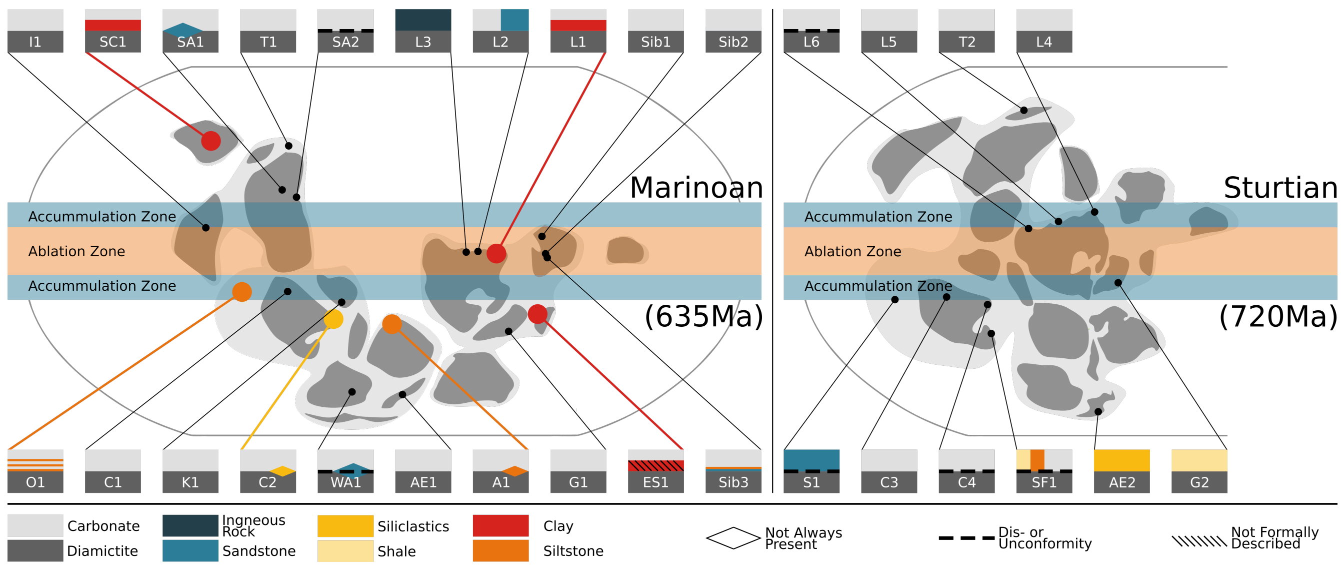

Supplementary Figure 4. Observed clay drapes
From 30 well-studied snowball Earth field sites for which detailed stratigraphic information is available or the boundaries between glacial and postglacial formations have explicitly been described, only two exhibit distinct clay deposits between the characteristic diamicite and overlying carbonate layers. One of these sites is located at the Marinoan paleoequator (L1), the other around 45° (SC1). One more occurrence of clay drapes, at around 30° (ES1), was reported, but never formally described in the peer reviewed literature. Thus, only one reported occurrence of a distinct clay layer can be placed within the latitudinal range that models identified as the tropical ablation zone, i.e. below 10°[2], while one, possibly two, occurrences are located even beyond the main accumulation zones that extend between roughly 10° and 20°. When assuming that dust might present itself as a thin siltstone layer or inter-bedded silt-carbonate structures, two more sites, at 15° (O1) and 30° (A1), may indicate pronounced dust-flushings during deglaciation, none of which likely occurred within the tropical ablation zone. Several studies have identified discrete ash depositions within the glacial stratifications and at least at one of these sites the ash presents itself as a widespread layer close to the glacial-postglacial boundary (C2). There are other instances where the diamicite is topped by either siltstone (SF1), shale (SF1, G2) or fine siliclastics (AE2); however in these instances the layers are very thick and there is no cap carbonate, making it extremely unlikely that they are the result of deglaciation dust-fluxes. While it is not impossible that in some instances clay layers went unreported, most of the studies either describe the boundary between diamicite and cap carbonate as very sharp or report the presence of other materials such as sandstone or ingneous rocks, making it unlikely that clay drapes were merely overlooked. Thus, if a hard snowball Earth ever existed, geological evidence does not strongly indicate the presence of extensive clay drapes, which suggests that a thick dust layer in the tropical ablation zone may not have occurred. Note that the above maps are based on Li et al. (2013)[3] and Hoffman et al. (2017)[4] and an overview over the reviewed publications is provided in the table 1.

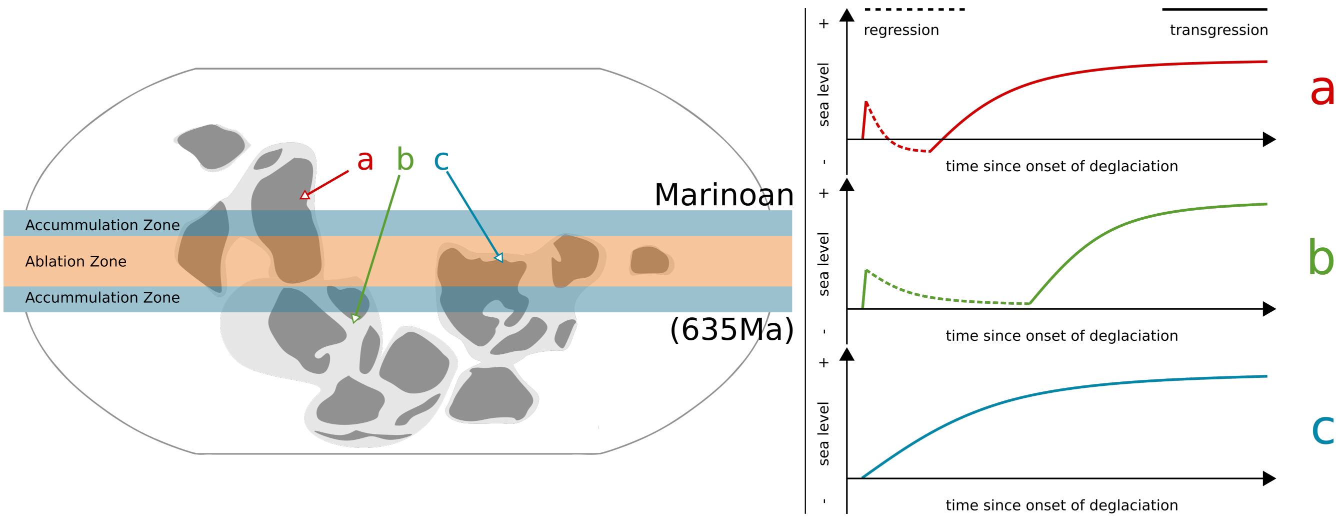

Supplementary Figure 5. **Post-glacial sea-level histories**
During the process of deglaciation, the combination of isostatic rebound and the reduced gravitational attraction of the shrinking ice-sheet lowers (relative) regional sea-levels. In the early stages of the deglaciation this relative decline could have offset the effect of the meltwater-induced global rise in sea-levels, resulting in a local regression[5]. In the case of a spatially-variable deglacation this would result in pronounced regional differences in the syndeglaciation sea-level curves. Regions with an early onset of deglaciation would show an initial regression followed by a transgression, while those regions where deglaciation starts relatively late exhibit a rise in sea-levels which is either continuous or interrupted by a regression at a later stage. For panels a-c, we adapted schematic sea-level curves from Creveling and Mitrovica (2014)[6], based upon stratigraphic sequences of the Marinoan deglaciation. Site a is an extratropical site located in present-day South Australia[7,8], site b a subtropical site on the Congo craton[5] and site c is located in the tropical ablation zone on the Laurentia craton[9] – the locations of the respective sites are indicated in the left panel of the figure. The post-glacial sea-level histories of these sites are consistent with (but not necessarily unique to) a deglaciation that was triggered outside of the tropical ablation zone, with both the extra-tropical sites showing an initial regression[7], consistent with the initiation of deglaciation in the mid-latitudes, whereas the tropical site merely shows a sustained transgression, consistent with a delayed onset of deglaciation[6,10]. However, a number of additional factors will modify when and where sea-level rises during the deglaciation and other potential reasons exist that could explain the particular sea-level histories, such as the sites' position relative to the neighboring continental ice sheet or spatial differences in ice sheet thickness. Thus a true test of our deglaciation-hypothesis requires a much more comprehensive knowledge of post-glacial sea levels including a better constraint on the relative timing of transgressive and regressive sequences.

Site	Lat.-Range [°]	Country	Craton	References
A1	25 - 35	Brazil (Paraguay Belt)	Amazonia	Alvarenga et al. (2004,2008,2011)[11–13]
AE1	55 - 65	Scotland	Avalonia (east)	McCay et al. (2006)[14]; Arnaud and Eyles (2006)[15]; Prave and Fallick (2011)[16]
AE2	60 - 70	Scotland	Avalonia (east)	McCay et al. (2006)[14];Arnaud and Eyles (2006)[15]; Prave and Fallick (2011)[16]
C1	15 - 25	Dem. Rep. of Congo	Congo	Master and Wendorf (2011)[17]
C2	25 - 35	Namibia	Congo	Hoffman et al. (1998,2011)[18,19]; Hoffmann et al. (2004)[20]; Prave et al. (2016)[21]
C3	15 - 25	Dem. Rep. of Congo	Congo	Master and Wendorf (2011)[17]
C4	20 - 30	Namibia	Congo	Le Heron et al. (2012)[22]
ES1	25 - 35	Norway (Svalbard)	East Svalbard	Halverson et al. (2004)[23], Abbot and Pierrehumbert (2010)[24]
G1	30 - 40	Greenland	Greenland	Stouge et al. (2011)[25]
G2	30 - 40	Greenland	Greenland	Stouge et al. (2011)[25]
I1	5 - 15	India	India	Jiang et al. (2003)[26]; Etienne et al.(2011)[27]
K1	25 - 35	Namibia/South Africa	Kalahari	Frimmel et al. (2002)[28]
L1	0 - 10	Canada	Laurentia	Hoffman and Halverson (2011)[9]
L2	0 - 10	Canada	Laurentia	McMechan (2000)[29]; Smith et al. (2011)[30]
L3	0 - 10	Canada	Laurentia	Kendall et al. (2004)[31]; Smith et al. (2011)[30]
L4	5 - 15	USA (Death Valley)	Laurentia	Prave (1999)[32]; Petterson et al. (2011)[33]; Macdonald et al. (2013)[34]
L5	5 - 15	USA (Idaho)	Laurentia	Fanning and Link (2004)[35]
L6	5 - 15	USA (Alaska)	Laurentia	Macdonald (2011)[36]
O1	10 - 20	Oman	Oman	Allen et al. (2004,2011)[37,38]; Kilner et al. (2005)[39]
S1	10 - 20	Ethiopia	Sahara	Miller et al. (2011)[40]
SA1	15 - 25	Australia	Southern Australia	Williams et al. (2008)[41]
SA2	15 - 25	Tasmania	Southern Australia	Hoffman et al. (2009)[42]; Calver et al. (2011,2013)[43,44]
SC1	40 - 50	China	South China	Zhang et al. (2008)[45]; Zhang et al. (2011)[46]; Hoffman and Li (2009)[47]
SF1	30 - 40	Brazil (Sao Francisco)	Sao Francisco	Uhlein et al. (1999,2011)[48,49]
Sib1	0 - 10	Siberia	Siberia	Sovetov (2011)[50]
Sib2	0 - 10	Siberia	Siberia	Chumakov (2011)[51]
Sib3	0 - 10	Siberia	Siberia	Chumakov (2011)[52]
T1	40 - 50	Mongolia	Tarim	Macdonald et al. (2009)[53]
T2	40 - 50	Mongolia	Tarim	Macdonald et al. (2009)[53]
WA1	55 - 65	Algeria/Mali	West Africa	Shields-Zhou et al. (2007,2011)[54,55]; Boudzoumou et al. (2011)[56]

Supplementary Table 1. Overview over the publications that were reviewed in order to identify snowball Earth field sites that feature distinct clay drapes at the glacial-postglacial boundary. The first column gives the identifier of the site and the second the approximate latitudinal position during deglaciation (based on Li et al. (2013)[3] and Hoffman et al. (2017)[4]). The third column indicates the country in which the site is located, while the fourth column indicates the craton and the last column the studies that were reviewed.

Supplementary References

1. Mauritsen, T. *et al.* Developments in the mpi-m earth system model version 1.2 (mpi-esm1.2) and its response to increasing co2. *Journal of Advances in Modeling Earth Systems* **11**, 998–1038 (2019). URL https://agupubs.onlinelibrary.wiley.com/doi/abs/10.1029/2018MS001400. https://agupubs.onlinelibrary.wiley.com/doi/pdf/10.1029/2018MS001400.

2. Abbot, D. S. *et al.* Robust elements of snowball earth atmospheric circulation and oases for life. *Journal of Geophysical Research: Atmospheres* **118**, 6017–6027 (2013). URL https://doi.org/10.1002/jgrd.50540.

3. Li, Z.-X., Evans, D. A. & Halverson, G. P. Neoproterozoic glaciations in a revised global palaeogeography from the breakup of rodinia to the assembly of gondwanaland. *Sedimentary Geology* **294**, 219–232 (2013). URL https://doi.org/10.1016/j.sedgeo.2013.05.016.

4. Hoffman, P. F. *et al.* Snowball earth climate dynamics and cryogenian geology-geobiology. *Science Advances* **3**, e1600983 (2017). URL https://doi.org/10.1126/sciadv.1600983.

5. Hoffman, P. & Macdonald, F. Sheet-crack cements and early regression in marinoan (635 ma) cap dolostones: Regional benchmarks of vanishing ice-sheets? *Earth and Planetary Science Letters* **300**, 374–384 (2010).

6. Creveling, J. R. & Mitrovica, J. X. The sea-level fingerprint of a snowball earth deglaciation. *Earth and Planetary Science Letters* **399**, 74 – 85 (2014). URL http://www.sciencedirect.com/science/article/pii/S0012821X14002696.

7. Rose, C. V. & Maloof, A. C. Testing models for post-glacial 'cap dolostone' deposition: Nuccaleena formation, south australia. *Earth and Planetary Science Letters* **296**, 165 – 180 (2010). URL http://www.sciencedirect.com/science/article/pii/S0012821X10002128.

8. Rose, C. V. *et al.* The end-cryogenian glaciation of south australia. *Geoscience Canada* **40**, 256–293 (2013). URL https://journals.lib.unb.ca/index.php/GC/article/view/20099.

9. Hoffman, P. F. & Halverson, G. P. Chapter 36 neoproterozoic glacial record in the mackenzie mountains, northern canadian cordillera. *Geological Society, London, Memoirs* **36**, 397–412 (2011). URL https://doi.org/10.1144/m36.36.

10. Creveling, J. R., Bergmann, K. D. & Grotzinger, J. P. Cap carbonate platform facies model, Noonday Formation, SE California. *GSA Bulletin* **128**, 1249–1269 (2016). URL https://doi.org/10.1130/B31442.1. https://pubs.geoscienceworld.org/gsabulletin/article-pdf/128/7-8/1249/3413362/1249.pdf.

11. de Alvarenga, C. J., Santos, R. V. & Dantas, E. L. C–o–sr isotopic stratigraphy of cap carbonates overlying marinoan-age glacial diamictites in the paraguay belt, brazil. *Precambrian Research* **131**, 1–21 (2004). URL https://doi.org/10.1016/j.precamres.2003.12.006.

12. de Alvarenga, C. J. *et al.* Isotope stratigraphy of neoproterozoic cap carbonates in the araras group, brazil. *Gondwana Research* **13**, 469–479 (2008). URL https://doi.org/10.1016/j.gr.2007.05.004.

13. Alvarenga, C. J. S. *et al.* Chapter 45 glacially influenced sedimentation of the puga formation, cuiabá group and jacadigo group, and associated carbonates of the araras and corumbá groups, paraguay belt, brazil. *Geological Society, London, Memoirs* **36**, 487–497 (2011). URL https://doi.org/10.1144/m36.45.

14. McCay, G., Prave, A., Alsop, G. & Fallick, A. Glacial trinity: Neoproterozoic earth history within the british-irish caledonides. *Geology* **34**, 909 (2006). URL https://doi.org/10.1130/g22694a.1.

15. Arnaud, E. & Eyles, C. H. Neoproterozoic environmental change recorded in the port askaig formation, scotland: Climatic vs tectonic controls. *Sedimentary Geology* **183**, 99–124 (2006). URL https://doi.org/10.1016/j.sedgeo.2005.09.014.

16. Prave, A. R. & Fallick, A. E. Chapter 63 the neoproterozoic glaciogenic deposits of scotland and ireland. *Geological Society, London, Memoirs* **36**, 643–648 (2011). URL https://doi.org/10.1144/m36.63.

17. Master, S. & Wendorff, M. Chapter 12 neoproterozoic glaciogenic diamictites of the katanga supergroup, central africa. *Geological Society, London, Memoirs* **36**, 173–184 (2011). URL https://doi.org/10.1144/m36.12.

18. Hoffman, P. F., Halverson, G. P., Schrag, D. P. & Kaufman, A. J. A neoproterozoic snowball earth. *Science* **281**, 1342–1346 (1998). URL https://doi.org/10.1126/science.281.5381.1342.

19. Hoffman, P. F. Chapter 2 a history of neoproterozoic glacial geology, 1871–1997. *Geological Society, London, Memoirs* **36**, 17–37 (2011). URL https://doi.org/10.1144/m36.2.

20. Hoffmann, K.-H., Condon, D., Bowring, S. & Crowley, J. U-pb zircon date from the neoproterozoic ghaub formation, namibia: Constraints on marinoan glaciation. *Geology* **32**, 817 (2004). URL https://doi.org/10.1130/g20519.1.

21. Prave, A. R., Condon, D. J., Hoffmann, K. H., Tapster, S. & Fallick, A. E. Duration and nature of the end-cryogenian (marinoan) glaciation. *Geology* **44**, 631–634 (2016). URL https://doi.org/10.1130/g38089.1.

22. Le Heron, D. P., Busfield, M. E. & Kamona, F. G. R. An interglacial on snowball earth? dynamic ice behaviour revealed in the chuos formation, namibia. *Sedimentology* **60**, 411–427 (2012). URL https://doi.org/10.1111/j.1365-3091.2012.01346.x.

23. Halverson, G. P., Maloof, A. C. & Hoffman, P. F. The marinoan glaciation (neoproterozoic) in northeast svalbard. *Basin Research* **16**, 297–324 (2004). URL https://doi.org/10.1111/j.1365-2117.2004.00234.x.

24. Abbot, D. S. & Pierrehumbert, R. T. Mudball: Surface dust and snowball earth deglaciation. *Journal of Geophysical Research* **115**, D03104 (2010). URL https://doi.org/10.1029/2009jd012007.

25. Stouge, S. *et al.* Chapter 56 neoproterozoic (cryogenian–ediacaran) deposits in east and north-east greenland. *Geological Society, London, Memoirs* **36**, 581–592 (2011). URL https://doi.org/10.1144/m36.56.

26. Jiang, G., Sohl, L. E. & Christie-Blick, N. Neoproterozoic stratigraphic comparison of the lesser himalaya (india) and yangtze block (south china): Paleogeographic implications. *Geology* **31**, 917 (2003). URL https://doi.org/10.1130/g19790.1.

27. Etienne, J. L. *et al.* Chapter 31 the blaini formation of the lesser himalaya, NW india. *Geological Society, London, Memoirs* **36**, 347–355 (2011). URL https://doi.org/10.1144/m36.31.

28. Frimmel, H., Fölling, P. & Eriksson, P. G. Neoproterozoic tectonic and climatic evolution recorded in the gariep belt, namibia and south africa. *Basin Research* **14**, 55–67 (2002).

29. McMechan, M. Vreeland diamictites - neoproterozoic glaciogenic slope deposits, rocky mountains, northeast british columbia. *Bulletin of Canadian Petroleum Geology* **48**, 246–261 (2000). URL https://doi.org/10.2113/48.3.246.

30. Smith, M. D., Arnaud, E., Arnott, R. & Ross, G. M. Chapter 37 the record of neoproterozoic glaciations in the windermere supergroup, southern canadian cordillera. *Geological Society, London, Memoirs* **36**, 413–424 (2011). URL https://doi.org/10.1144/m36.37.

31. Kendall, B. S., Creaser, R. A., Ross, G. M. & Selby, D. Constraints on the timing of marinoan "snowball earth" glaciation by 187re–187os dating of a neoproterozoic, post-glacial black shale in western canada. *Earth and Planetary Science Letters* **222**, 729–740 (2004). URL https://doi.org/10.1016/j.epsl.2004.04.004.

32. Prave, A. R. Two diamictites, two cap carbonates, two Δ13c excursions, two rifts: The neoproterozoic kingston peak formation, death valley, california. *Geology* **27**, 339 (1999). URL https://doi.org/10.1130/0091-7613(1999)027<0339:tdtcct>2.3.co;2.

33. Petterson, R., Prave, A. R., Wernicke, B. P. & Fallick, A. E. The neoproterozoic noonday formation, death valley region, california. *Geological Society of America Bulletin* **123**, 1317–1336 (2011). URL https://doi.org/10.1130/b30281.1.

34. Macdonald, F. A. *et al.* The Laurentian record of Neoproterozoic glaciation, tectonism, and eukaryotic evolution in Death Valley, California. *GSA Bulletin* **125**, 1203–1223 (2013). URL https://doi.org/10.1130/B30789.1. https://pubs.geoscienceworld.org/gsabulletin/article-pdf/125/7-8/1203/3715813/1203.pdf.

35. Fanning, C. M. & Link, P. K. U-pb SHRIMP ages of neoproterozoic (sturtian) glaciogenic pocatello formation, southeastern idaho. *Geology* **32**, 881 (2004). URL https://doi.org/10.1130/g20609.1.

36. Macdonald, F. A. Chapter 34 the hula hula diamictite and katakturuk dolomite, arctic alaska. *Geological Society, London, Memoirs* **36**, 379–388 (2011). URL https://doi.org/10.1144/m36.34.

37. Allen, P. A., Leather, J. & Brasier, M. D. The neoproterozoic fiq glaciation and its aftermath, huqf supergroup of oman. *Basin Research* **16**, 507–534 (2004). URL https://doi.org/10.1111/j.1365-2117.2004.00249.x.

38. Allen, P. A. *et al.* Chapter 20 the abu mahara group (ghubrah and fiq formations), jabal akhdar, oman. *Geological Society, London, Memoirs* **36**, 251–262 (2011). URL https://doi.org/10.1144/m36.20.

39. Kilner, B., Niocaill, C. & Brasier, M. Low-latitude glaciation in the neoproterozoic of oman. *Geology* **33**, 413 (2005). URL https://doi.org/10.1130/g21227.1.

40. Miller, N. R., Avigad, D., Stern, R. J. & Beyth, M. Chapter 21 the tambien group, northern ethiopia (tigre). *Geological Society, London, Memoirs* **36**, 263–276 (2011). URL https://doi.org/10.1144/m36.21.

41. Williams, G. E., Gostin, V. A., McKirdy, D. M. & Preiss, W. V. The elatina glaciation, late cryogenian (marinoan epoch), south australia: Sedimentary facies and palaeoenvironments. *Precambrian Research* **163**, 307–331 (2008). URL https://doi.org/10.1016/j.precamres.2007.12.001.

42. Hoffman, P. F., Calver, C. R. & Halverson, G. P. Cottons breccia of king island, tasmania: Glacial or non-glacial, cryogenian or ediacaran? *Precambrian Research* **172**, 311–322 (2009). URL https://doi.org/10.1016/j.precamres.2009.06.003.

43. Calver, C. R. Chapter 64 neoproterozoic glacial deposits of tasmania. *Geological Society, London, Memoirs* **36**, 649–658 (2011). URL https://doi.org/10.1144/m36.64.

44. Calver, C. *et al.* Globally synchronous marinoan deglaciation indicated by u-pb geochronology of the cottons breccia, tasmania, australia. *Geology* **41**, 1127–1130 (2013). URL https://doi.org/10.1130/g34568.1.

45. Zhang, S., Jiang, G. & Han, Y. The age of the nantuo formation and nantuo glaciation in south china. *Terra Nova* **20**, 289–294 (2008). URL https://doi.org/10.1111/j.1365-3121.2008.00819.x.

46. Zhang, Q.-R., Chu, X.-L. & Feng, L.-J. Chapter 32 neoproterozoic glacial records in the yangtze region, china. *Geological Society, London, Memoirs* **36**, 357–366 (2011). URL https://doi.org/10.1144/m36.32.

47. Hoffman, P. F. & Li, Z.-X. A palaeogeographic context for neoproterozoic glaciation. *Palaeogeography, Palaeoclimatology, Palaeoecology* **277**, 158–172 (2009). URL https://doi.org/10.1016/j.palaeo.2009.03.013.

48. Uhlein, A., Trompette, R. R. & Alvarenga, C. J. Neoproterozoic glacial and gravitational sedimentation on a continental rifted margin: The jequitai–macaubas sequence (minas gerais, brazil). *Journal of South American Earth Sciences* **12**, 435–451 (1999). URL https://doi.org/10.1016/s0895-9811(99)00032-2.

49. Uhlein, A., Alvarenga, C. J. S., Dardenne, M. A. & Trompette, R. R. Chapter 51 the glaciogenic jequitaí formation, southeastern brazil. *Geological Society, London, Memoirs* **36**, 541–546 (2011). URL https://doi.org/10.1144/m36.51.

50. Sovetov, J. K. Chapter 28 late cryogenian (vendian) glaciogenic deposits in the marnya formation, oselok group, in the foothills of the east sayan range, southwestern siberian craton. *Geological Society, London, Memoirs* **36**, 317–329 (2011). URL https://doi.org/10.1144/m36.28.

51. Chumakov, N. M., Pokrovsky, B. G. & Melezhik, V. A. Chapter 27 the glaciogenic bol'shoy patom formation, lena river, central siberia. *Geological Society, London, Memoirs* **36**, 309–316 (2011). URL https://doi.org/10.1144/m36.27.

52. Chumakov, N. M. Chapter 25 glacial deposits of the nichatka formation, chara river basin and review of upper precambrian diamictites of central siberia. *Geological Society, London, Memoirs* **36**, 297–302 (2011). URL https://doi.org/10.1144/m36.25.

53. Macdonald, F. A., Jones, D. S. & Schrag, D. P. Stratigraphic and tectonic implications of a newly discovered glacial diamictite–cap carbonate couplet in southwestern mongolia. *Geology* **37**, 123–126 (2009). URL https://doi.org/10.1130/g24797a.1.

54. Shields, G. A. *et al.* Neoproterozoic glaciomarine and cap dolostone facies of the southwestern taoudéni basin (walidiala valley, senegal/guinea, NW africa). *Comptes Rendus Geoscience* **339**, 186–199 (2007). URL https://doi.org/10.1016/j.crte.2006.10.002.

55. Shields-Zhou, G. A., Deynoux, M. & Och, L. Chapter 11 the record of neoproterozoic glaciation in the taoudéni basin, NW africa. *Geological Society, London, Memoirs* **36**, 163–171 (2011). URL https://doi.org/10.1144/m36.11.

56. Boudzoumou, F., Vandamme, D., Affaton, P. & Gattacceca, J. Neoproterozoic paleomagnetic poles in the taoudeni basin (west africa). *Comptes Rendus Geoscience* **343**, 284–294 (2011). URL https://doi.org/10.1016/j.crte.2010.12.001.